Materials Chemistry and Physics 137 (2013) 689–693

Contents lists available at SciVerse ScienceDirect

Materials Chemistry and Physics

journal homepage: www.elsevier.com/locate/matchemphys

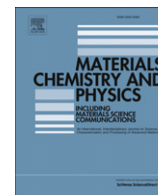

Review

How tantalum proceeds phase change on tantalum nitride underlayer with sequential Ar plasma treatment

Jung-Chih Tsao [a], Chuan-Pu Liu [a], Hsin-Chiao Fang [a], Ying-Lang Wang [b,*]

[a] Department of Materials Science and Engineering, National Cheng Kung University, Tainan 701, Taiwan, ROC
[b] College of Photonics, National Chiao Tung University, Tainan, Taiwan, ROC

HIGHLIGHTS

► The sequential Ta film phase transitions from β-Ta to α-Ta on TaN after Ar treatment.
► The treatment makes β-Ta (202) plane lattice atoms arrange to α-Ta with close packed lattice atoms at (110) planes.
► β-Ta/amorphous-TaN microstructure transits to a composite of α-Ta/bcc-Ta(N) and amorphous-TaN mixture stacking layers.

ARTICLE INFO

Article history:
Received 27 March 2012
Received in revised form
7 August 2012
Accepted 22 September 2012

Keywords:
Tantalum
Argon bombardment
TaN
Phase transformation

ABSTRACT

Tantalum can change its phase from high resistive β-Ta to low resistive α-Ta phase on a TaN substrate with sequential Ar plasma treatment on the TaN layer surface prior to Ta deposition. The underlined mechanism of phase evolution is proposed based on systematic microstructure examination by high-resolution transmission electron microscopy. The images show that, with argon treatment, the upper part of the TaN film is transformed from amorphous-TaN to a composite phase of bcc-Ta(N) and amorphous-TaN mixture, which is also confirmed by X-ray diffraction patterns. The composite film composed of less nitrogen provides an ideal cubic matrix to confine the stable α-Ta phase to be grown. The α-Ta/bcc-Ta(N) film obtained by proper argon treatment results in film resistivity 10 times lower than the traditional Ta/TaN film.

© 2012 Elsevier B.V. All rights reserved.

1. Introduction

Tantalum (Ta) thin film possesses diverse properties and has been widely applied in semiconductor industry for microelectronic devices [1–4]. Especially, Ta could form two crystalline phases, each exhibiting vastly different electrical properties. One is a stable body-centered cubic (bcc) α-Ta phase, with resistivity between 20 and 30 μΩ-cm, while the other is a metastable tetragonal β-Ta phase, with higher resistivity of 180–220 μΩ-cm [5–7]. The metastable β-Ta phase is the most commonly formed phase during magnetron sputtering due to high levels of gaseous impurities [6–8].

A TaN underlayer is one of the choices to act as a nucleation layer for α-Ta. However, the bottom TaN layer is a complex compound with many possible phases, depending on the composition ratio of Ta to N. Therefore, the Ta film could be induced to form β-Ta, α-Ta or mixture [9,10]. The resulting resistance can vary in the range of 80 (Ta-rich film) to 350 μΩ-cm (N-rich film) [4,6,7].

Given the aforementioned benefits, previous researches have proposed to overcome the challenge of forming low resistive α-Ta on amorphous TaN by inserting an argon treatment with magnetron sputtering [11,12] that provides a great amount of ionized energy to change surface conditions [13]. This is a facile method to control Ta phase, and thus low resistivity film, by applying argon treatment on the TaN layer surface prior to Ta deposition. However, the underlined mechanism of phase evolution is still not known.

Therefore, in this study we examine the phase evolution of both Ta and TaN with amount of argon bombardment by high resolution transmission electron microscopy (HRTEM) and propose a mechanism responsible for phase transformation. We also demonstrate that the bilayer structure with best film **non-uniformity** can be achieved.

2. Experimental

In this study, the fabrication of the Ta/treated-TaN bilayer consists of three steps as shown in Fig. 1(a). All depositions were performed at room temperature and the base pressure better than 1×10^{-7} torr was reached prior to sputtering. Firstly, a TaN layer

* Corresponding author. Tel.: +886 6 5051400x3031; fax: +886 6 5051273.
E-mail address: ylwang@tsmc.com (Y.-L. Wang).

0254-0584/$ – see front matter © 2012 Elsevier B.V. All rights reserved.
http://dx.doi.org/10.1016/j.matchemphys.2012.09.053

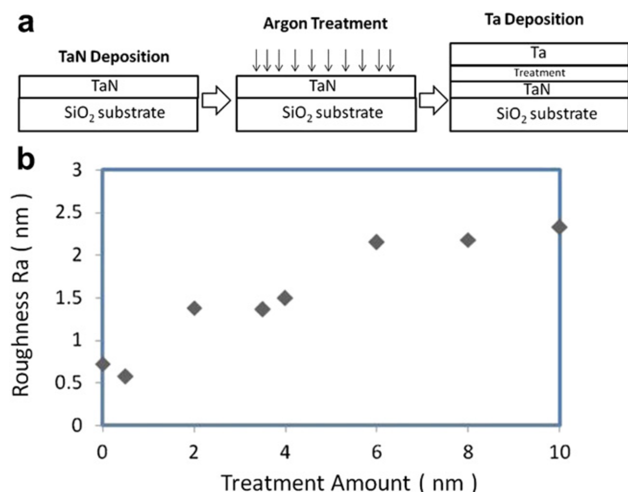

Fig. 1. (a) Schematic diagram of the fabrication flow for the Ta/treated-TaN barrier layer with growth interruption for argon bombardment treatment. (b) The argon treatment amount and TaN surface roughness correlation.

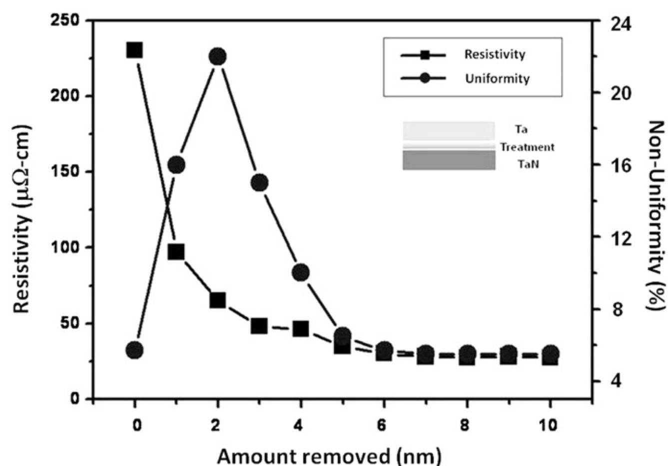

Fig. 2. Electrical resistivity of the Ta/treated-TaN barrier and its **non-uniformity** as a function of amount removed by argon treatment at the interface.

was deposited on the substrate by reactive sputtering using an Ar flow of 50 sccm mixed with a N_2 gas at a flux of 23 sccm. Secondly, surface treatment by argon bombardment was applied by an RF plasma source with a power up to 1200 W at 13.56 MHz. Finally, a Ta layer was deposited on top using only Ar. A DC power of 20 kW was employed for both Ta and TaN deposition. For fair comparison, the thickness of the Ta layer was fixed at ~20 nm, while that of the TaN layer after argon treatment was kept at ~14 nm for all conditions employed.

Sheet resistance with its **non-uniformity** was measured by a KLA-Tencor four point probe measurement station, RS-100. Thickness was measured by a picosecond ultrasonic laser sonar methodology with Rudolph Technologies MetaPULSE [14,15]. The sheet resistance **non-uniformity** within wafer is given below.

$$\text{Non}-\text{uniformity}\,\% = (\text{standard deviation}/\text{mean})\%$$

Crystal structure of the bilayers was determined by glancing angle X-ray diffraction (XRD) with Rigaku D/MAX2500. Cross-sectional microstructure was examined by HRTEM with a JEOL 2100F operating at 200 keV. To protect layer structure from damage during TEM sample preparation, a ~20 nm SiN layer was deposited on top as a cap layer. In addition, TEM samples were prepared by hand polishing, dimpling, and ion milling to perforation. The TEM images were interpreted by Fourier transform and analyzed by CaRIne Crystallography 3.1 software [16] to obtain the phases.

3. Results and discussion

The argon bombardment on TaN increases nanoscale surface roughness Ra. As shown in Fig. 1(b), Ra is 0.5 nm from the as-deposited TaN film and then steadily increases to about 2.3 nm after the film removed for 10 nm by bombardment.

Fig. 2 is the electric property of the bilayer structure with different TaN amounts removed by argon treatment at the interface. Apparently, the pristine bilayer without interface treatment exhibits high resistivity of 235 μΩ-cm and resistivity decreases exponentially with TaN amount removed until saturation at the minimum resistivity of 30 μΩ-cm for 6 nm treatment. On the other hand, argon treatment degrades the resistivity **non-uniformity** within wafer significantly for small amounts of TaN removed, which reaches the poorest **non-uniformity** of **23%** for 2 nm treatment. Upon more TaN amounts removed, resistivity **non-uniformity** also improves rapidly and reaches the best **non-uniformity** of **4.5%** for 6 nm treatment. Obviously, we demonstrate that surface treatment through argon ion bombardment on the TaN layer prior to the Ta layer deposition exerts a huge impact on the resistivity of the Ta/TaN bilayer, implying that phase transition might have occurred.

To verify the crystal structure, XRD results are shown in Fig. 3(a) for the pristine high resistive Ta/TaN bilayer without interface treatment and Fig. 3(b) for the low resistive Ta/treated-TaN with the TaN film removed for 8 nm. The two figures reveal the common feature of a broadened peak for TaN, suggestive of amorphous or nanocrystalline TaN phase. The results also indicate that, without treatment, β-Ta forms as shown in Fig. 3(a) with the preferential growth along <202>. If treated properly, the phase transforms to α-Ta in Fig. 3(b) with the preferential growth changed to <110>. However, if considering lattice mismatch, the relative peak shift of the TaN to the β-Ta (202) is 0.31° in Fig. 3(a), which is less than that of 0.91° in Fig. 2(b) for the TaN relative to the α-Ta (110). By examining the TaN peak in Fig. 3(b) more closely, the peak is asymmetry and a small peak at 38.42° can be identified, which corresponds to bcc-Ta(N). The peak shift of the bcc-Ta(N) to the α-Ta (110) is 0.05° only, which implies that the atomic structure of TaN has been modified to facilitate the nucleation of the α-Ta phase. Since the peak is too weak, this has to be verified by TEM characterization later.

Obviously, derived from the above discussion, lattice matching via modifying the atomic structure of the underlayer is important in governing the phase change of the Ta layer. Fig. 4(a1) and (b1) exhibit the unit cell of β-Ta in tetragonal and α-Ta in cubic, respectively, whereas Fig. 4(a2) and (b2) compare the atomic structure of β-Ta (202) and α-Ta (110) as the most prevalent planes, respectively. The symmetry, spacing and stacking of atoms are drastically distinct between them. The atoms in Fig. 4(a2) and (b2) form a basic unit from parallelogram to rectangle with different characteristic side lengths, to which the underlayer should match.

Fig. 5 shows TEM images of the bilayer structure without and with interface argon treatment for 8 nm. Obviously, the treatment process results in an additional transition region at the interface between Ta and TaN exhibiting brighter contrast in Fig. 5(b) for the treated sample compared to the untreated structure in Fig. 5(a) where such contrast is absent.

In order to investigate the bilayer microstructure in detail, high magnification images were performed and shown in Fig. 6. Fig. 6(a)

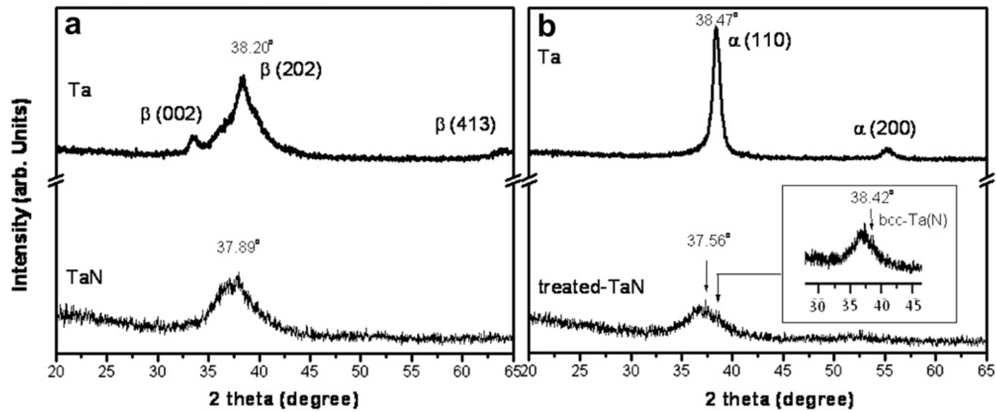

Fig. 3. X-ray diffraction spectra of the as-deposited Ta layer and TaN underlayer (a) without interface treatment (b) with argon treatment 8 nm on TaN prior to Ta deposition.

presents a bright field cross-sectional TEM image of the pristine Ta/TaN layer without interface treatment. Fig. 6(b) is the diffraction pattern of the entire bilayer and proves that the Ta layer is β-phase and the TaN layer is amorphous. Fig. 6(c) and (d) show the corresponding lattice images of the marked area from the Ta and TaN layer in Fig. 6(a), respectively. In Fig. 6(c), the most prominent interplanar spacings are identified to be 2.40 Å and 2.35 Å as indicated, which correspond to {202} and {330} planes of β-Ta, respectively, in agreement with the results from Fig. 6(b). In Fig. 6(d), the TaN layer is demonstrated to be amorphous, which is also confirmed by the power spectrum in the inset and agrees with the previous results under similar growth conditions at room temperature [6]. Hence, based on the above analysis, the Ta/TaN layer without any growth interruptions for argon treatment shows the structure being β-Ta formed on an amorphous-TaN layer.

On the other hand, Fig. 7(a) shows the HRTEM image of the treated Ta/TaN bilayer. Apparently, contrast variation suggests the presence of three layers across the layers including an interfacial layer between Ta and TaN. Fig. 7(b) shows the diffraction pattern of the Ta layer, indicating that the layer is polycrystalline, corresponding to α-Ta phase. Fig. 7(c), (d) and (e) show the HRTEM lattice images of the Ta, interfacial, and TaN layer, respectively, as marked in Fig. 7(a). The inset in each image is the corresponding FFT pattern. In Fig. 7(c), the interplanar spacing is identified to be 2.338 Å and agrees with α-Ta (110) plane. Besides, in Fig. 7(d), the lattice spacing is 2.383 Å, which corresponding to Ta(N) (110) plane.

Fig. 7(e) reveals that the TaN layer is composed of amorphous phase at the bottom and bcc-Ta(N) phase on top upon argon bombardment. As a result, we demonstrate that the crystal structure of the underlying TaN layer is crucial for the phase of the subsequent Ta layer. Through ion bombardment, α-Ta can be effectively induced on amorphous TaN with the surface structure being modified to crystalline bcc structure. The surface composition ratio of N to Ta has also been confirmed to decrease from 50.70% to 45.95% after the surface treatment by X-ray photoelectron spectroscopy.

From all the aforementioned results, the growth scenario of how the argon treatment can induce α-Ta can be rationalized as a set of

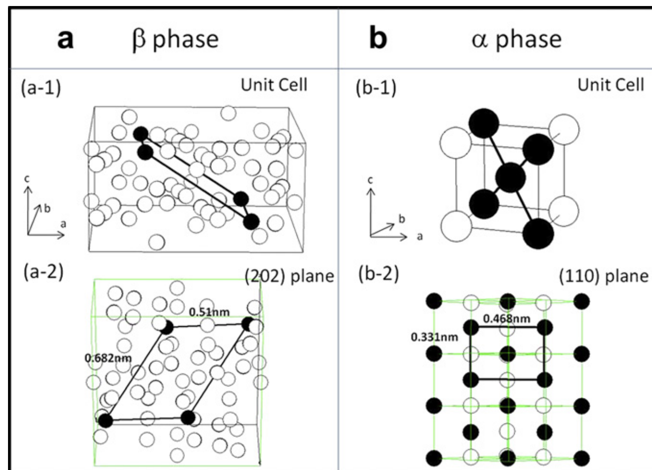

Fig. 4. Structure illustration of (a1) β-phase unit cell, (a2) β-phase (202) atomic structure, (b1) α-Ta unit cell, and (b2) α-Ta (110) atomic structure.

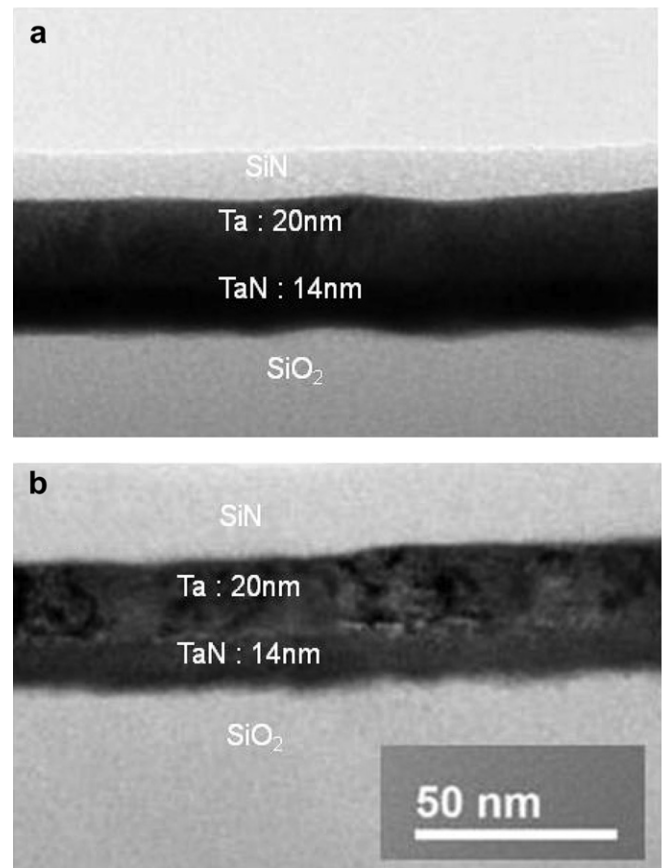

Fig. 5. Low-magnification cross-sectional TEM images of the Ta/TaN bilayer structure (a) without interface treatment (b) with argon treatment 8 nm on TaN prior to Ta deposition.

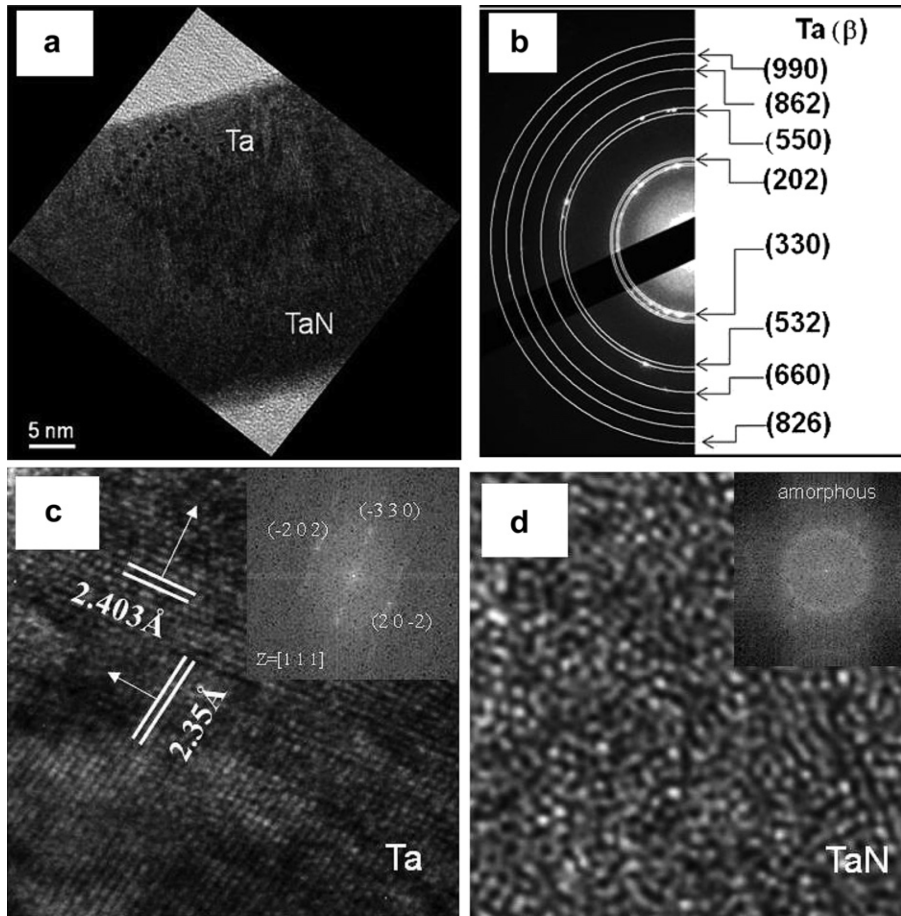

Fig. 6. (a) High magnification bright-field TEM image of the untreated Ta/TaN layer as in Fig. 4a: (b) Electron diffraction pattern of the Ta layer; and high resolution TEM images of (c) the Ta (d) Tthe TaN layer from the regions indicated in (a), with the insets showing the corresponding fast Fourier transform (FFT) patterns.

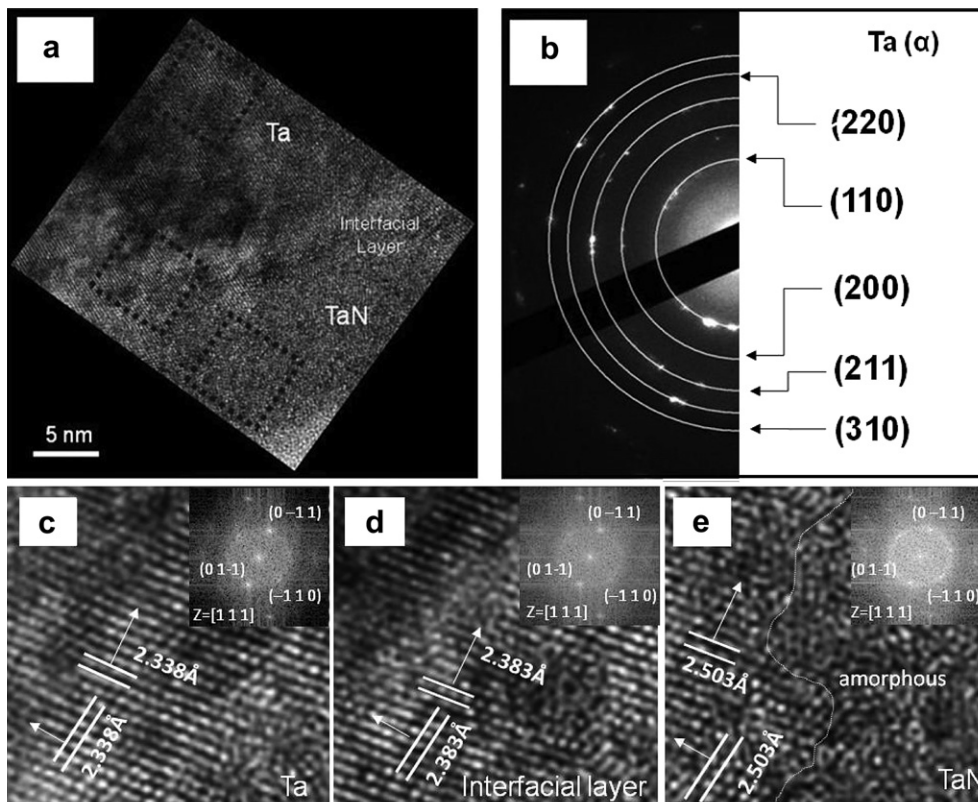

Fig. 7. (a) High magnification bright-field TEM image of the treated Ta/TaN layer as in Fig. 2b: (b) Electron diffraction pattern of the Ta layer; and high resolution TEM images of (c) the Ta (d) the interfacial (e) the TaN layer from the regions indicated in (a), with the insets showing the corresponding FFT patterns.

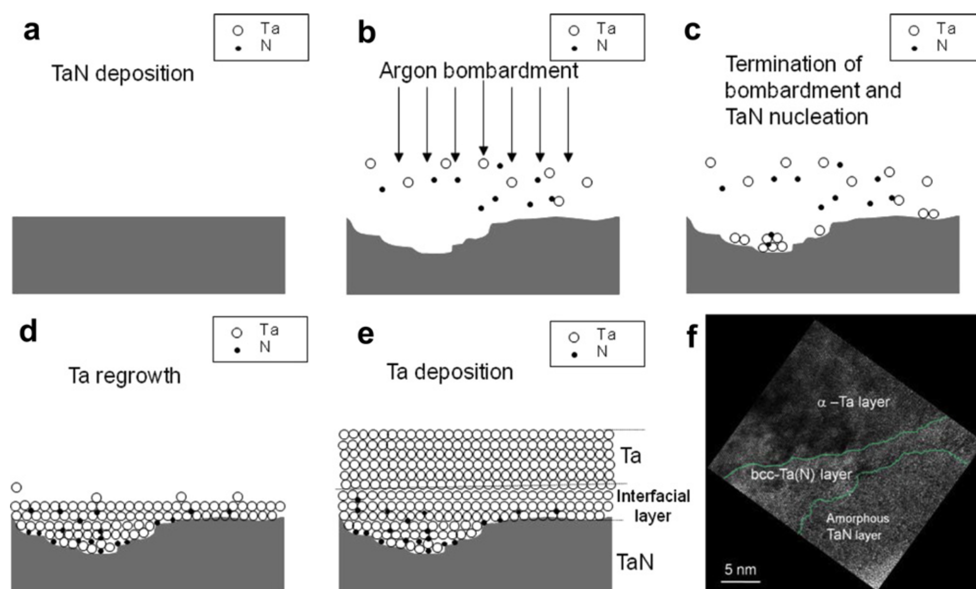

Fig. 8. Schematic diagrams of the growth mechanisms of the Ta/treated-TaN layer with argon treatment (a) TaN deposition (b) argon bombardment (c) TaN island nucleation (d) TaN regrowth (e) Ta deposition (f) TEM image of the as-deposited two layer for comparison.

schematic diagrams in Fig. 8. First, an amorphous TaN layer was deposited at room temperature in Fig. 8(a). Subsequently, argon bombardment onto the TaN surface results in a roughened surface as shown in Fig. 8(b). When the resputtering process stops, the residual gases containing TaN molecules and dissociated Ta atomic species redeposit preferentially on surface concave regions as in Fig. 8(c). Dissociated nitrogen species can be pumped out preferentially, leading to a metal like Ta(N) cubic phase to form as in Fig. 8(d). This is the key stage where the accumulation of these small Ta clusters is likely to form as the bulk-like (bcc) structure, which is characterized by its stability [17]. Finally, as shown in Fig. 8(e), an α-Ta layer can be induced on the ideal cubic Ta(N) underlayer due to minimum lattice mismatch of 0.8% between bcc-Ta(N) {110} and α-Ta {110}. The entire structure with the optimal configuration can now be achieved as shown in Fig. 8(f).

4. Conclusions

In this study, a treatment process by argon bombardment to the TaN layer was applied prior to the Ta layer deposition. It was found that the optimum treatment amount is related to the formation of cubic Ta(N) phase on top of the as-deposited TaN film. The HRTEM images show that, upon ion bombardment, the stoichiometric amorphous TaN phase in the upper region of the TaN layer was changed to the bcc-Ta(N), which provides the minimum lattice mismatch to promote the α-Ta overlayer formation.

Acknowledgments

The work was supported by Research Grant NSC-98-2221-E-006-079-MY3, National Science Council of Taiwan.

References

[1] Q. Xie, X.P. Qu, J.J. Tan, Y.L. Jiang, M. Zhou, T. Chen, G.P. Ru, Appl. Surf. Sci. 253 (2006) 1666.
[2] K.L. Ou, W.F. Wu, C.P. Chou, S.Y. Chiou, C.C. Wu, J. Vac. Sci. Technol. B 20 (2002) 2154.
[3] K.H. Min, K.C. Chun, K.B. Kim, J. Vac. Sci. Technol. B 14 (1996) 3263.
[4] J.C. Tsao, C.P. Liu, Y.L. Wang, K.W. Chen, J. Nanosci. Nanotechnol 8 (2008) 2582.
[5] A. Jiang, A. Yohannan, N.O. Nnolim, T.A. Tyson, L. Axe, S.L. Lee, P. Cote, Thin Solid Films 437 (2003) 116.
[6] J.W. Lim, M. Mimura, M. Isshiki, Jpn. J. Appl. Phys. 43 (2004) 8267.
[7] P. Gregory, A.J. Bangay, T.L. Bird, Metallurgia 71 (1965) 207.
[8] C.S. Seet, B.C. Zhang, C. Yong, S.L. Liew, K. Li, L.C. Hsia, H.L. Seng, T. Osipowicz, J. Sudijono, H.C. Zeng, J.B. Tan, J. Electrochem. Soc. 150 (2003) G766.
[9] S.M. Rossnagel, J. Vac. Sci. Technol. B 20 (2002) 2328.
[10] H. Donohue, J.C. Yeoh, K. Giles, K. Buchanan, Micr. Eng. 64 (2002) 299.
[11] Y.S. Wang, W.H. .Lee, Y.L. .Wang, C.C. .Hung, S.C. Chang, J. Phys. Chem. Solids 69 (2008) 601.
[12] K.W. Chen, Y.L. Wang, J.C. Tsao, K.Y. Lo, J. Nanosci, Nanotechnology 8 (2008) 2500.
[13] E.M. Lee, W.C. Shin, Y.S. Choi, S.G. Yoon, J. Electrochem. Soc. 148 (2001) G611.
[14] C. Thomsen, H.T. Grahn, H.J. Maris, J. Tauc, Phys. Rev. B 34 (1986) 4129.
[15] C.J. Morath, G.J. Collins, R.G. Wolf, R.J. Stoner, Solid State Technol. 40 (1997) 85.
[16] C. Boudias, D. Monceau, CaRIne Crystallography 3.1 © (1989) (1998).http://pro.wanadoo.fr/carine.crystallography.
[17] A. Jiang, T.A. Tyson, L. .Axe, J. Phys. Condens. Matter 17 (2005) 6111.